

## Achieving C–N bond cleavage in dinuclear metal cyanide complexes†

Germán Cavigliasso,<sup>a</sup> Gemma J. Christian,<sup>a</sup> Robert Stranger<sup>\*a</sup> and Brian F. Yates<sup>b</sup>

Received 10th February 2011, Accepted 18th May 2011

DOI: 10.1039/c1dt10225g

Cleavage of cyanide is more difficult to achieve compared to dinitrogen and carbon monoxide, even though these species contain triple bonds of greater strength. In this work, we have used computational methods to investigate thermodynamic and mechanistic aspects of the C–N bond cleavage process in  $[L_3M-CN-M'L_3]$  systems consisting of a central cyanide unit bound in an end-on fashion to two terminal metal tris-amide complexes. In these systems,  $[M]$  is a  $d^3$  transition metal from the 3d, 4d, 5d, or 6d series and groups 4 through 7, and  $[L]$  is either  $[NH_2]$ ,  $[NMe_2]$ ,  $[N^iPrPh]$ , or  $[N^iBuAr]$ . A comparison of various models for the experimentally relevant  $[L_3Mo-CN-MoL_3]$  system has shown that while the C–N cleavage step appears to be an energetically favourable process, a large barrier exists for the dissociation of  $[L_3Mo-CN-MoL_3]^{(-)}$  into  $[L_3Mo-C]^{(-)}$  and  $[N-MoL_3]$ , which possibly explains why C–N bond scission is not observed experimentally. The general structural, bonding, and thermochemical trends across the transition metal series investigated, indicate that the systems exhibiting the greatest degree of C–N activation, and most favourable energetics for C–N cleavage, also possess the most favourable electronic properties, namely, a close match between the relevant  $\pi$ -like orbitals on the metal-based and cyanide fragments. The negative charge on the cyanide fragment leads to significant destabilization of the  $\pi^*$  level which needs to be populated through back-donation from the metal centres in order for C–N bond scission to be achieved. Therefore, metal-based systems with high-lying  $d_x$  orbitals are best suited to C–N cleavage. In terms of chemical periodicity, these systems can be identified as the heavier members within a group and the earlier members within a period. As a consequence, Mo complexes are not well suited to cleaving the C–N bond, whereas the Ta analogues are the most favourable systems and should, in principle, be capable of cleaving cyanide under relatively mild conditions. An important conclusion from this work is that a successful strategy for achieving cleavage of multiply-bonded, and relatively unreactive, molecular fragments, may simply lie in tuning the electronic structures and orbital interactions by judicious choice of metal sites and ligand groups.

## 1 Introduction

Interest in metal-cyanide chemistry<sup>1–5</sup> stems from the “broad availability of cyanide complexes involving the transition elements and the diverse chemical and physical properties that make these systems attractive in many areas of chemical research (for example, materials science, organometallic compounds, biological and medicinal chemistry) and for a variety of applications (such

as nanostructures, electrochromism, molecular magnetism, and molecular electronics)”.<sup>1</sup>

In connection with the general problems of molecular functionalization and synthesis of species exhibiting multiple metal-element bonding, activation and scission of the C–N bond is of particular interest since experimental and computational research<sup>6,7</sup> has shown that cleavage of cyanide using metal complexes is considerably more difficult to achieve compared to dinitrogen and carbon monoxide, even though these diatomic molecules contain triple bonds of greater strength. In the case of cyanide, its negative charge leads to destabilization of the  $\pi^*$  level that needs to be populated through back-donation from the metal atoms in order for C–N bond scission to be achieved. Consequently, metal complexes that are capable of cleaving dinitrogen may not necessarily be well suited to cleaving cyanide.

Scission of the C–N bond in organometallic iron–cyano species has been reported by Fehlhammer and coworkers,<sup>8</sup> but the reaction does not lead to metal–carbide and metal–nitride products. In this system, the anionic dinuclear iron–cyano complex (*cis*- $[Fe_2(CN)Cp_2(\mu-CO)_2(CO)]^-$ ) reacts with phthaloyl dichloride to

<sup>a</sup>Australian National University Research School of Chemistry, Canberra, ACT 0200, Australia

<sup>b</sup>University of Tasmania School of Chemistry, Hobart, TAS 7001, Australia

† Electronic supplementary information (ESI) available. Figures and tables containing:

- Potential energy scans for the dissociation of the dinuclear species into carbide and nitride products, in the  $[L_3Nb-CN-NbL_3]$  and  $[L_3Ta-CN-TaL_3]$  ( $L = [NH_2]$ ) systems.
- Comparison of the influence of the solvent model (toluene or water) and ligand ( $L = NH_2$  or  $L = NMe_2$ ) on the energy gaps between the relevant  $\pi$ -like  $[\Delta E(\pi)]$  fragment orbitals in  $[L_3M-CN-M'L_3]$  ( $L = NH_2$ ) species.
- Comparison of results from gradient-corrected (Becke–Perdew) and hybrid (B3-LYP) functional calculations for Mo and Ta ( $L = NH_2$ ) systems. See DOI: 10.1039/c1dt10225g



Approximation (ZORA)<sup>31–33</sup> and the Conductor-like Screening Model (COSMO) was used for the treatment of solvation effects,<sup>34</sup> with water as the solvent. Calculations were performed in a spin-unrestricted manner using default convergence parameters, whose values are  $10^{-3}$  hartree for energy,  $10^{-2}$  hartree/angstrom for gradients, and 4.0 for the integration accuracy. Frequency calculations were carried out using numerical approaches<sup>35,36</sup> with an integration accuracy of 6.0. Temperature and pressure values used in free energy results were 298.15 K and 1.0 atm, respectively. Plots of the molecular orbitals were generated with the MOLEKEL program<sup>37,38</sup> using data in MOLDEN format<sup>39,40</sup> derived from the ADF-TAPE21 files.

For comparative purposes, additional calculations have been carried out for selected systems using the B3-LYP hybrid functional,<sup>41</sup> and these results are given in the supplementary sections. The most important observation, in the context of the current study, is that the Becke–Perdew and B3-LYP calculations give qualitatively similar energetic trends. It should be noted that although in some cases quantitative differences are found, these results have also been reported for analogous metal–dinitrogen systems<sup>42</sup> and do not significantly affect the overall conclusions.

### 3 Results and discussion

Cummins and coworkers have attempted to achieve scission of the C–N bond in metal–cyanide systems through a variety of experimental procedures.<sup>6</sup> Their initial strategy involved the reaction of  $[\text{Mo}(\text{NRAr})_3]$ —where  $\text{R} = [\text{C}(\text{CD}_3)_2\text{CH}_3]$  and  $\text{Ar} = [3,5\text{-C}_6\text{H}_3\text{Me}_2]$ —with  $[\text{N}^n\text{Bu}_4][\text{CN}^-]$ , which yielded a mononuclear  $[\text{Mo}–\text{CN}]$  species characterized as  $[\text{N}^n\text{Bu}_4][\text{NC}–\text{Mo}(\text{NRAr})_3]$ . However, subsequent reactions leading to the formation of the cyanide-bridged di-molybdenum complex or the carbide and nitride products, which would provide evidence that the C–N bond has been cleaved, were not observed.

A different strategy was successful in preparing an uncharged dinuclear species, corresponding to  $[(\text{NRAr})_3\text{Mo}–\text{CN}–\text{Mo}(\text{NRAr})_3]$ , but subsequent reduction with  $[\text{Na}/\text{Hg}]$  amalgam resulted in ejection of an  $[\text{R}]$  group instead of formation of  $[(\text{NRAr})_3\text{Mo}–\text{CN}–\text{Mo}(\text{NRAr})_3]^{(-)}$ , despite this species being iso-electronic with a neutral dinitrogen analogue that does undergo cleavage of the N–N bond leading to  $[\text{N}–\text{Mo}(\text{NRAr})_3]$  products.<sup>9,10</sup>

It is important to note that, although cleavage of the C–N bond through a process involving a cyanide-bridged dinuclear metal species has not been achieved experimentally, the eventual products of this reaction, namely the metal–carbide and metal–nitride species, have been independently synthesized in the case where the starting reagent is  $[\text{Mo}(\text{NRAr})_3]$ .<sup>10,14</sup> Furthermore, the successful synthesis and structural characterization of a dinuclear mixed-metal  $[\text{Mo}–\text{CN}–\text{V}]$  complex has been reported.<sup>6</sup>

#### 3.1 Comparison of $[\text{N}–\text{N}]$ , $[\text{C}–\text{O}]$ , and $[\text{C}–\text{N}]$ species

Experimental attempts to cleave synthetically important multiply-bonded diatomic molecules such as  $\text{N}_2$ ,  $\text{CO}$ , and  $\text{CN}^-$ , using  $[\text{Mo}(\text{NRAr})_3]$  complexes, have only been successful in the dinitrogen case. All of these species possess strong triple bonds, as confirmed by the following experimental dissociation energy results,

$$\text{C}–\text{O} = 1076 \text{ kJ mol}^{-1}$$

$$\text{N}–\text{N} = 945 \text{ kJ mol}^{-1}$$

$$\text{C}–\text{N}^- = 887 \text{ kJ mol}^{-1}$$

Nevertheless, our computational investigations<sup>7,20</sup> have shown that, despite the strength of the bonding interactions clearly being an important factor, it is the energy match between relevant  $\pi$ -like orbitals on the metal-based and small molecule fragments that appears to play the central role in the activation and cleavage process. This requirement can be rationalized on the basis that the principal mechanism for bond scission involves back-donation from the metal-based  $d_\pi$  levels into the  $\pi^*$  antibonding levels of the small molecule.

The following comparison of relevant  $\pi$ -like orbital energy gaps in  $[\text{L}_3\text{M}–\text{X}^1\text{X}^2–\text{M}'\text{L}_3]$  ( $\text{L} = \text{NH}_2$ ) complexes of dinitrogen, carbon monoxide, and cyanide, using metal atoms with d-electron configurations optimized for cleavage of the relevant small molecule,<sup>18</sup>

$$\text{Re} [\text{C}–\text{O}] \text{Ta} = 4.20 \text{ eV}$$

$$\text{Mo} [\text{N}–\text{N}] \text{Mo} = 1.61 \text{ eV}$$

$$\text{Re} [\text{C}–\text{N}^-] \text{W} = 6.51 \text{ eV}$$

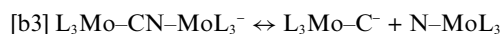
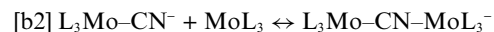
shows that although cyanide possesses the weakest bonding interactions, the energy match between the metal-based  $d_\pi$  and small-molecule  $\pi^*$  orbitals is poorest, implying that C–N bond scission is more difficult to achieve than cleavage of the N–N and C–O bonds.

#### 3.2 Computational results for $[\text{Mo}–\text{CN}–\text{Mo}]$ systems

Given the experimental relevance of  $[\text{Mo}(\text{NRAr})_3]$  complexes, we have undertaken calculations on three molybdenum–cyanide model systems containing amide ligands of increasing size and complexity, namely,  $[\text{NH}_2]$ ,  $[\text{NMe}_2]$ , and  $[\text{N}^i\text{PrPh}]$ . Additional calculations have been carried out on the actual experimental system, which corresponds to  $[\text{N}^i\text{BuAr}]$ , but we have only been able to obtain limited results as a consequence of the much greater computational effort required for this species.

Calculations for the  $[\text{NH}_2]$  case were constrained to  $C_{3v}$  symmetry in order to avoid problems encountered during geometry optimizations, which typically lead to the formation of unrealistic structures that cannot be regarded as representative of the actual species, due to the presence of hydrogen bonding or excessive geometric distortion. As these issues do not apply to the  $[\text{NMe}_2]$  and  $[\text{N}^i\text{PrPh}]$  cases, no constraints were imposed and all calculations were performed in  $C_1$  symmetry.

Reaction profiles were obtained using the following scheme



and a comparison of results for the three model systems is presented in Fig. 1.

Irrespective of the identity of the amide ligand, the calculations predict that the overall reaction should be exothermic but that the cleavage step from the dinuclear species to the carbide and nitride products, along the lowest energy path, is not favourable. These results are in agreement with previous computational studies that were limited to  $[\text{NH}_2]$  ligand systems.<sup>7</sup>

It is interesting to note that, although the exothermicity of the overall reaction is considerably smaller for the  $[\text{N}^i\text{PrPh}]$  ( $-121 \text{ kJ mol}^{-1}$ ) compared to  $[\text{NMe}_2]$  ( $-258 \text{ kJ mol}^{-1}$ ) and  $[\text{NH}_2]$  ( $-249 \text{ kJ mol}^{-1}$ ) systems, no clear correlation with the differences in ligand size has been found. Instead, an energy decomposition analysis suggests that a combination of changes in steric (Pauli

repulsion), electrostatic, orbital, and solvation effects is associated with the calculated variations in overall exothermicity.

Plots of the optimized structures of the dinuclear species for the three ligand systems are given in Scheme 1. Also included are the values of the C–N distance, which can be used as a measure of bond activation, and the metal–cyanide (M–C–N and N–C–M) bond angles for the  $C_1$  optimized structures. The calculated C–N separation in the isolated cyanide ion is 118 pm, and therefore a relatively significant degree of C–N activation, ranging from 7 to 11 pm, is observed in the dinuclear species for all three ligand systems.

The calculated values can also be correlated with the extent of distortion of the central  $[\text{Mo}–\text{C}–\text{N}–\text{Mo}]$  core. The shortest C–N distance is found in the  $[\text{NH}_2]$  system, in which linearity of

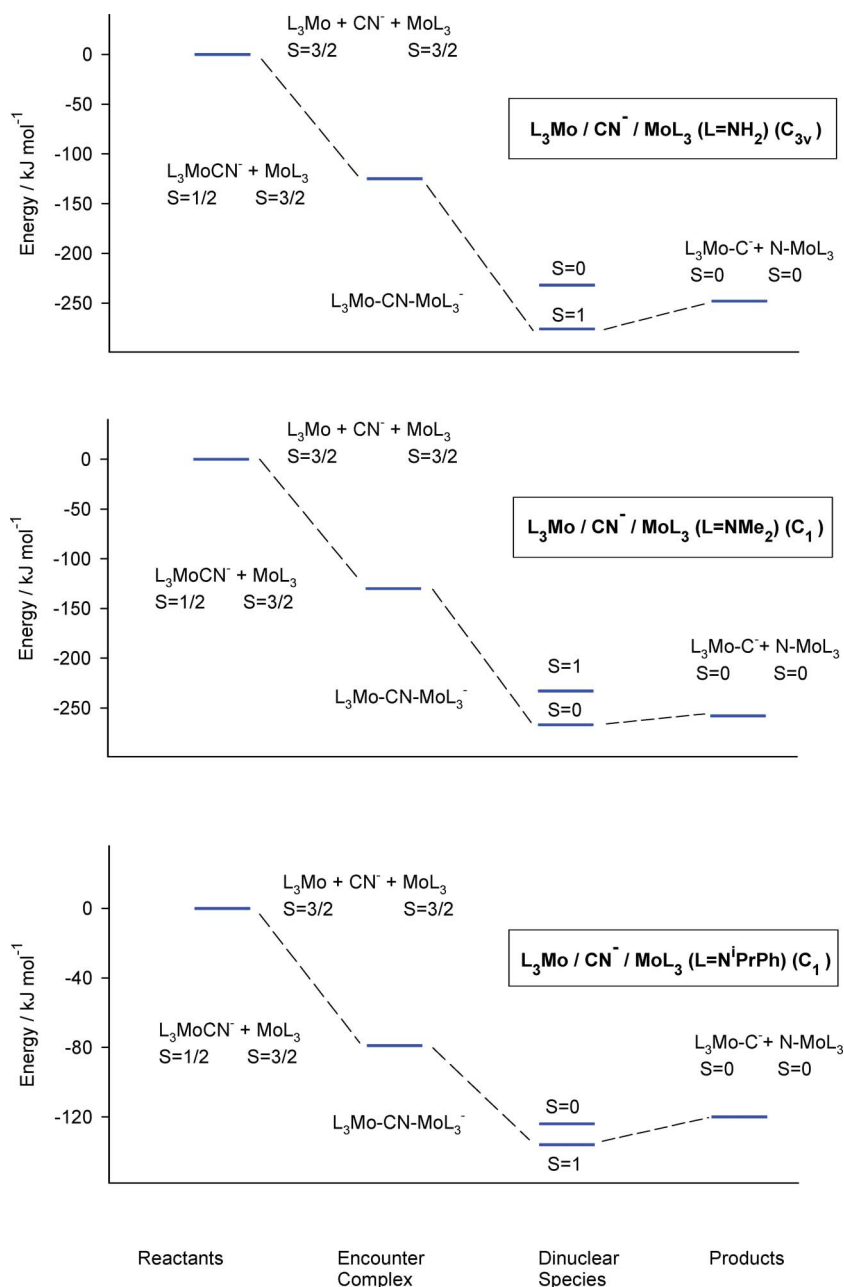
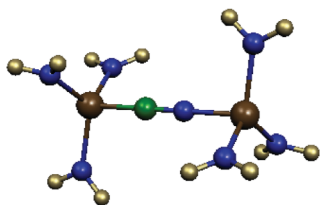


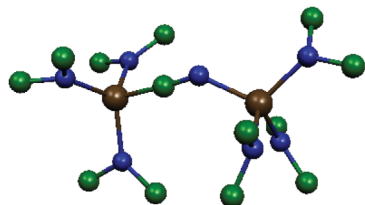
Fig. 1 Comparison of reaction energy profiles for  $[\text{Mo}–\text{CN}–\text{Mo}]$  systems.

$[\text{L}_3\text{Mo-CN-MoL}_3]^{(-)}$ ,  $\text{L}=\text{NH}_2$  ( $S=1$ ) ( $C_{3v}$ , symmetry)



C-N = 125.0 pm

$[\text{L}_3\text{Mo-CN-MoL}_3]^{(-)}$ ,  $\text{L}=\text{NMe}_2$  ( $S=0$ ) ( $C_1$  symmetry)

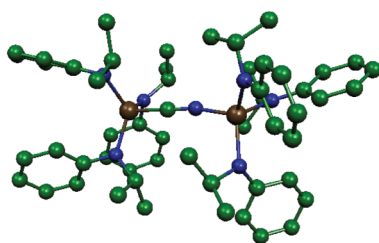


C-N = 128.8 pm

MoCN = 177°

CNMo = 135°

$[\text{L}_3\text{Mo-CN-MoL}_3]^{(-)}$ ,  $\text{L}=\text{N}^i\text{PrPh}$  ( $S=1$ ) ( $C_1$  symmetry)



C-N = 126.3 pm

MoCN = 177°

CNMo = 168°

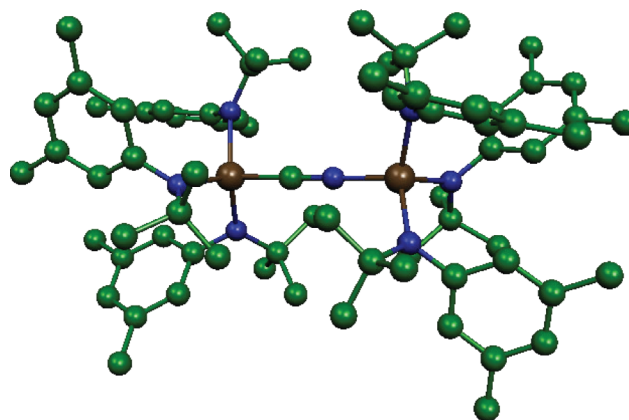
Scheme 1

the [Mo-CN-Mo] core is enforced. A somewhat more activated C-N bond is predicted for the [NMe<sub>2</sub>] system compared with the [N<sup>i</sup>PrPh] analogue, which exhibits a smaller distortion (from linearity) presumably due to the more significant steric constraints imposed by the larger isopropyl and phenyl ligand fragments in the latter. It is also interesting to note that the M-C-N and N-C-M bond angles calculated for  $[(\text{N}^i\text{PrPh})_3\text{Mo-CN-Mo}(\text{N}^i\text{PrPh})_3]^{(-)}$  are similar to those observed in the experimentally characterized [Mo-CN-V] complex.<sup>6</sup>

A full geometry optimization of  $[(\text{N}^i\text{BuAr})_3\text{Mo-CN-Mo}(\text{N}^i\text{BuAr})_3]^{(-)}$  indicates that the [Mo-CN-Mo] core in this structure should be almost exactly linear, as shown in Scheme 2. This result correlates with the fact that both experimental characterization and computational modelling of the molybdenum-dinitrogen ( $(\text{N}^i\text{BuAr})_3\text{Mo-NN-Mo}(\text{N}^i\text{BuAr})_3$ ) analogue have revealed the presence of a linear [Mo-NN-Mo] core in this species.<sup>43,44</sup> In a general sense, the observed tendency towards adoption of a linear configuration of the central moiety in this type of dinuclear metal system is consistent with the necessity of minimizing steric repulsion as the size and volume of the organic groups in the amide ligands increase.

A noteworthy similarity between the [NH<sub>2</sub>] and [N<sup>i</sup>PrPh] systems is that, in both cases, the more stable form of the dinuclear

$[\text{L}_3\text{Mo-CN-MoL}_3]^{(-)}$ ,  $\text{L}=\text{N}^i\text{BuAr}$  ( $S=1$ ) ( $C_1$  symmetry)



C-N = 126.8 pm

MoCN = 179°

CNMo = 179°

Scheme 2

species corresponds to the spin triplet state, unlike the [NMe<sub>2</sub>] system, for which the spin singlet state is favoured. These results can be related to the fact that in  $[(\text{N}^i\text{PrPh})_3\text{Mo-CN-Mo}(\text{N}^i\text{PrPh})_3]^{(-)}$  the central [Mo-CN-Mo] core is reasonably close to linearity, which in  $[(\text{NH}_2)_3\text{Mo-CN-Mo}(\text{NH}_2)_3]^{(-)}$  is necessarily imposed by the  $C_{3v}$  symmetry. In contrast, the large geometric distortions in the [NMe<sub>2</sub>] analogue, which involve significant bending of the [Mo-CN-Mo] axis and rotation of the amide ligands, lead to inversion of the singlet and triplet states, as previously observed for the  $C_{2h}$  form of  $[(\text{NH}_2)_3\text{Mo-NN-Mo}(\text{NH}_2)_3]$  compared to its  $D_{3d}$  counterpart.<sup>44,45</sup>

**3.2.1 Free energy analysis.** Since the results contained in Fig. 1 only provide an indication of enthalpic effects, we have undertaken additional calculations in order to estimate the entropic contributions and construct overall free energy reaction profiles. These calculations were performed for the [NH<sub>2</sub>] and [NMe<sub>2</sub>] systems but not for the [N<sup>i</sup>PrPh] case, due to the large size of the dinuclear  $[(\text{N}^i\text{PrPh})_3\text{Mo-CN-Mo}(\text{N}^i\text{PrPh})_3]^{(-)}$  species rendering the relevant numerical frequency procedures (which are required for a complete thermochemical analysis) unfeasible for this system.

The free energy reaction profiles for the [NH<sub>2</sub>] and [NMe<sub>2</sub>] systems are given in Fig. 2. The stoichiometry associated with the dissociation of the dinuclear species into products implies that entropic effects should favour C-N cleavage and formation of the carbide and nitride species. The calculations predict that the entropic contribution is sufficiently large to counteract the unfavourable enthalpic effects and render the dissociation step energetically favourable by 10 and 55 kJ mol<sup>-1</sup> in the case of [NH<sub>2</sub>] and [NMe<sub>2</sub>] systems, respectively.

**3.2.2 Formation of the dinuclear species.** Although the focus of our investigation lies in the C-N bond cleavage step, it is also of interest to examine the formation of the dinuclear cyanide-bridged metal complexes for the two cases that have been

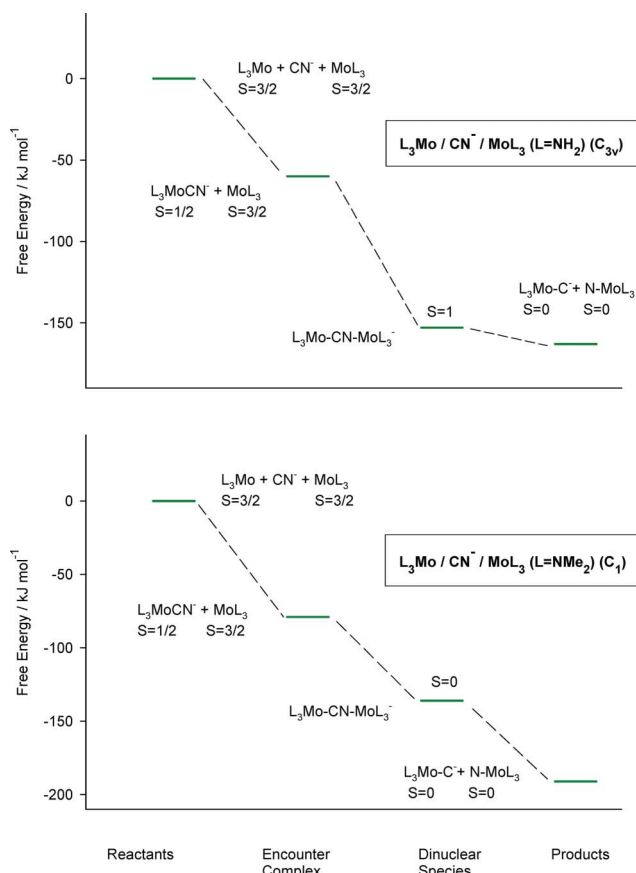
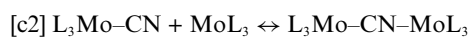


**Fig. 2** Comparison of reaction free energy profiles for [Mo–CN–Mo] systems.

experimentally explored, corresponding to the anionic and neutral systems represented by equations [c1] and [c2], respectively,



A comparison of energy profiles and potential energy scans for these two processes is given in Fig. 3, for the [NH<sub>2</sub>] case. In both the anionic and neutral cases, formation of the dinuclear species is predicted to be clearly favourable—although somewhat more exothermic for the latter than the former—and no barrier has been found along the respective potential energy curves, which show that the most favourable pathways correspond to spin triplet ( $\text{L}_3\text{Mo-CN-MoL}_3^-$ ) and doublet ( $\text{L}_3\text{Mo-CN-MoL}_3$ ) states.

The calculation of potential energy curves and transition states is considerably more complicated or impractical if large ligands are used, but it is reasonable to assume that the general qualitative features of the [NH<sub>2</sub>] system should also apply in more realistic cases. Thus, a possible explanation for the fact that the dinuclear species has been detected in neutral, but not anionic, conditions may lie in experimental difficulties associated with the preparation and characterization of the negatively charged structures.<sup>6</sup>

**3.2.3 Cleavage step.** As discussed in preceding sections, the results obtained in the [NH<sub>2</sub>] case using  $C_{3v}$  symmetry appear to be a satisfactory approximation to the behaviour of larger more realistic models such as the [N<sup>i</sup>PrPh] system, and they

may also be valid for the actual experimental species, for which computational modelling suggests that the [N<sup>i</sup>(Bu)Ar] ligands impose even greater spatial constraints that lead to adoption of a linear [Mo–CN–Mo] core. On the basis of these results, C–N bond cleavage in molybdenum–cyanide complexes, *via* a dinuclear intermediate species with an approximately linear [Mo–CN–Mo] moiety, appears to be feasible on the basis of relative free energy considerations.

However, the reaction profiles shown in Fig. 1 and 2 indicate that spin crossover from a triplet to singlet curve is required for the dissociation of the dinuclear species into the carbide and nitride products, since the triplet state is favoured for the former whereas the latter are most stable in the singlet state. Additional calculations for the [NH<sub>2</sub>] systems, which involved performing a potential energy scan for the dissociation of [(NH<sub>2</sub>)<sub>3</sub>Mo–CN–Mo(NH<sub>2</sub>)<sub>3</sub>]<sup>(+)</sup> into [(NH<sub>2</sub>)<sub>3</sub>Mo–C]<sup>(+)</sup> and [N–Mo(NH<sub>2</sub>)<sub>3</sub>] (shown in Fig. 4), suggest that a rather significant barrier of approximately 240 kJ mol<sup>-1</sup> is associated with the spin crossover from triplet to singlet curves and, thus, for C–N bond scission along the predicted lowest energy path.

Although calculations using relatively high symmetry may provide a satisfactory approximation to the structure and energetics of stable species in the reaction profile, it is possible that the relevant transition states adopt more distorted geometric configurations that are not adequately described within  $C_{3v}$  symmetry constraints. Accordingly, reaction barriers have also been estimated for the [NH<sub>2</sub>] system using  $C_s$  symmetry, and in this case a significantly smaller value of 110 kJ mol<sup>-1</sup> was obtained. However, the geometric distortion occurring in the corresponding transition state structure appears excessively large to be representative of the experimental system. Consequently, the most appropriate description may lie at an intermediate point between the  $C_s$  and  $C_{3v}$  results, but probably closer to the latter, and thus a significant barrier to C–N bond cleavage is likely to exist. This observation is confirmed by results obtained for the [N<sup>i</sup>PrPh] model system, which indicate that the magnitude of the barrier is 53 kJ mol<sup>-1</sup> smaller than in the  $C_{3v}$  [NH<sub>2</sub>] case, but 79 kJ mol<sup>-1</sup> greater than that predicted by the  $C_s$  [NH<sub>2</sub>] calculation (Fig. 4).

The presence of a considerable barrier in the cleavage step may explain why, under experimental conditions, other reactions are observed instead of the carbide and nitride products resulting from scission of the C–N bond. In the molybdenum–cyanide system, the reluctance for C–N bond scission may be a consequence of the fact that the Mo atoms in the dinuclear intermediate species are not well suited, on the basis of their electronic structure, to ensure that C–N cleavage is dominant over other competing reactions.<sup>7</sup> This observation is consistent with the results of our computational study of trends in M–X bond strength,<sup>18</sup> which has revealed that Mo atoms in a formal +3 oxidation state—with an associated d<sup>3</sup> electronic configuration—are not ‘optimized’ for metal–carbon multiple bonding. Nevertheless, this problem could be resolved by modifying relevant properties, such as fragment orbital interactions, through the use of other metal combinations. This strategy is explored and discussed in the sections that follow.

### 3.3 Trends across transition metal series

In order to investigate the effect of changing the metal identity and overall molecular charge on the reaction energetics of

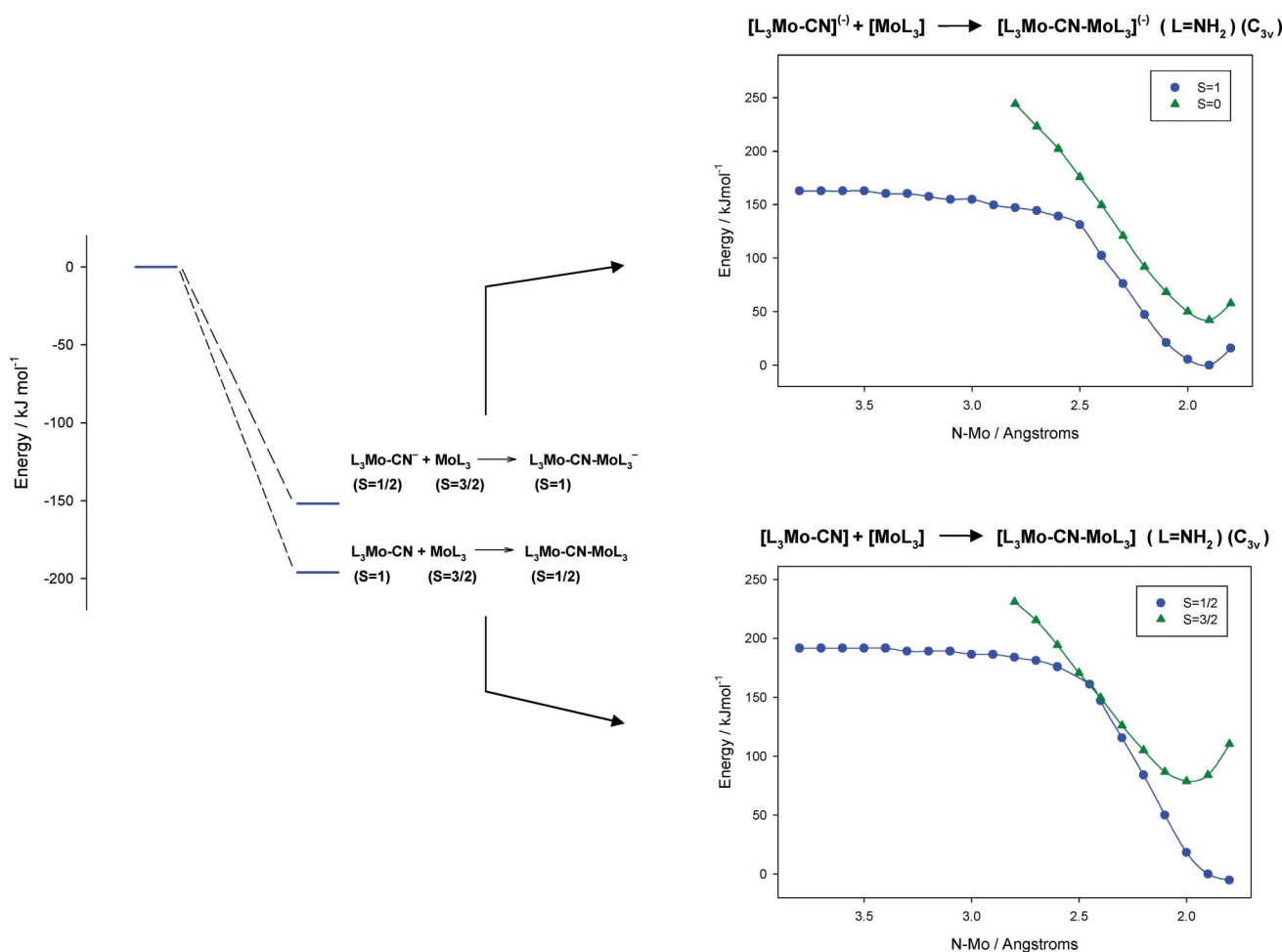


Fig. 3 Comparison of energy profiles and potential energy scans for the formation of the dinuclear species in anionic and neutral [Mo-CN-Mo] systems.

**Table 1** Interatomic distance of the cyanide unit (C-N in pm) in  $[L_3M-CN]$  ( $L = NH_2$ ) species in the doublet ( $S = 1/2$ ) spin state. Results correspond to  $C_{3v}$  symmetry

Metal Element	Molecular Charge	C-N <sup>a</sup>
Tc	0	119.0
Re	0	119.8
Bh	0	120.6
Cr	-1	119.8
Mo	-1	121.0
W	-1	122.4
Sg	-1	123.5
V	-2	123.5
Nb	-2	124.7
Ta	-2	126.7
Ti	-3	128.6

<sup>a</sup> Calculated C-N distance in isolated cyanide ion is 118 pm

C-N activation and cleavage by  $[ML_3]$  complexes, calculations were undertaken on a set of  $[NH_2]$  systems from all transition metal series (including the 6d elements) and groups 4 through 7. The general results, including structural, thermochemical, and bonding data, are summarized in Tables 1 through 4.

In all cases, the molecular symmetry was constrained to  $C_{3v}$  to ensure that the dinuclear structures satisfactorily approximate

the (quasi) linear  $[M-CN-M]$  configuration found in the more complex models and experimental systems. A relatively high symmetry is also necessary to undertake a detailed analysis of fragment orbital interactions, in particular, the separation of  $\sigma$  and  $\pi$  components.

The overall charge of the systems is determined by the fact that the formal electronic configuration of the metal atoms in the  $[ML_3]$  complexes has been chosen as  $d^3$  for all cases included in this study. This restriction is based on our earlier work,<sup>18</sup> which has shown that this d-electron configuration generates the strongest bonds between the metal atoms and  $[C]^{(-)}$  or  $[N]$  fragments in the products, thereby maximizing their stability and the thermodynamic driving force for the overall reaction.

Since most species along the reaction path are negatively charged, and in particular the dinuclear structures can possess a rather high charge, the solvation treatment employed in the calculations was chosen with the main purpose of providing adequate stabilization of these charged species. However, since properties such as metal-ligand orbital interactions can be particularly sensitive to the solvation environment,<sup>46,47</sup> tests were conducted in order to investigate both ligand and solvent effects on the orbital energy gaps. The relevant results, which are provided in the supplementary data, show that the general trends are not affected by changes in the ligand identity or solvation model.

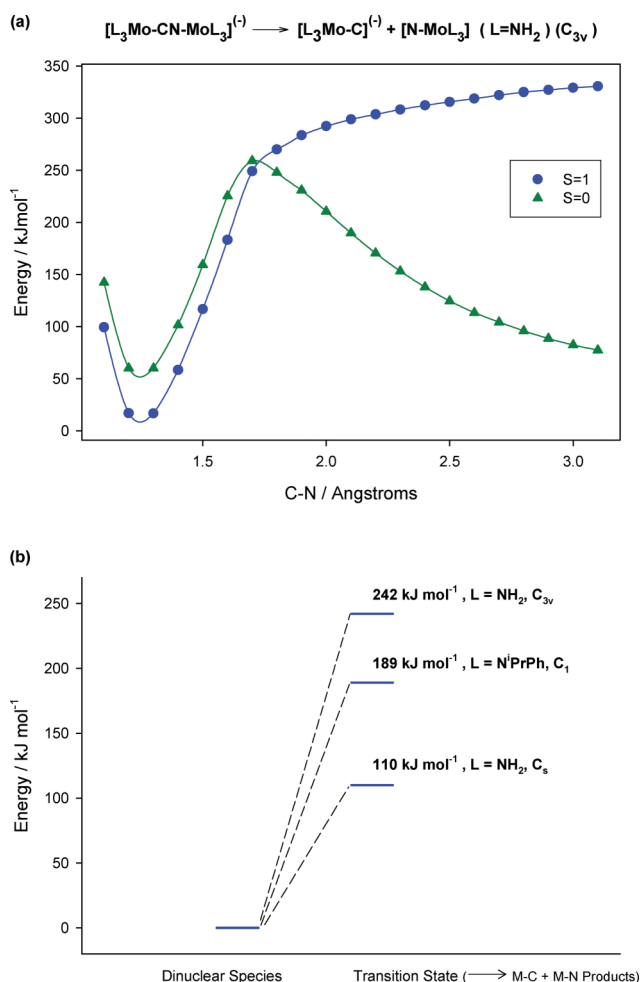


**Fig. 4** Potential energy scans for the dissociation of the dinuclear species into carbide and nitride products in the  $[\text{L}_3\text{M}-\text{CN}-\text{M}'\text{L}_3]^{(\pm)}$  ( $\text{L} = [\text{NH}_2]$ ) system (a) and comparison of barrier to C–N cleavage in  $[\text{NH}_2]$ ,  $[\text{NMe}_2]$ , and  $[\text{N}^i\text{PrPh}]$  systems (b).

**3.3.1 Structural and thermochemical trends.** As mentioned in the analysis of the  $[\text{NH}_2]$ ,  $[\text{NMe}_2]$ , and  $[\text{N}^i\text{PrPh}]$  systems presented in Section 3.2, the change in the interatomic distance associated with a given bond is typically used as a means of quantifying the degree of activation of that bond, and the relevant results for the metal–cyanide systems studied in this work are given in Table 1, for the encounter complex, and Table 2, for the dinuclear species.

For the  $[\text{L}_3\text{M}-\text{CN}]$  encounter complexes, the spin doublet ( $S = 1/2$ ) state is more favourable than the spin quartet ( $S = 3/2$ ) state, with the exception of the Ti and Cr systems. However, in these two systems, the energetic difference between the two spin states is small and therefore, for consistency, the results in Table 1 are only given for the  $S = 1/2$  case.

Compared to the calculated value of 118 pm for the C–N distance in the isolated cyanide ion, all  $[\text{L}_3\text{M}-\text{CN}]$  complexes studied exhibit an elongated C–N bond and, therefore, some degree of C–N activation. However, clear trends are observed within both groups and periods, namely, an increase in the C–N distance as a group is descended, and towards the earlier members across a given transition series. Thus, for the Tc species (from the 4d series and group 7) the C–N distance is only ~1 pm longer than

**Table 2** Interatomic distance of the cyanide unit (C–N in pm) in  $[\text{L}_3\text{M}-\text{CN}-\text{M}'\text{L}_3]$  ( $\text{L} = \text{NH}_2$ ) species. Results correspond to  $C_{3v}$  symmetry

Metal Elements	Molecular Charge	Spin State	C–N <sup>a</sup>
Tc, Mo	0	$S = 0$	122.9
		$S = 1$	122.3
Re, W	0	$S = 0$	124.2
		$S = 1$	123.6
Bh, Sg	0	$S = 0$	125.2
		$S = 1$	124.7
Cr, Cr	–1	$S = 0$	123.5
		$S = 1$	123.5
Mo, Mo	–1	$S = 0$	125.0
		$S = 1$	125.0
W, W	–1	$S = 0$	126.7
		$S = 1$	126.7
Sg, Sg	–1	$S = 0$	127.9
		$S = 1$	127.8
V, V	–3	$S = 0$	129.2
		$S = 1$	129.5
Nb, Nb	–3	$S = 0$	130.6
		$S = 1$	130.2
Ta, Ta	–3	$S = 0$	134.3
		$S = 1$	133.9
Ti, Ti	–5	$S = 0$	135.2
		$S = 1$	135.6

<sup>a</sup> Calculated C–N distance in isolated cyanide ion is 118 pm.

**Table 3** Comparison of thermochemical parameters ( $\Delta E$  = Bonding energy in  $\text{kJ mol}^{-1}$ ,  $\Delta G$  = Free energy in  $\text{kJ mol}^{-1}$ ) for the overall reaction ( $\text{R} \rightarrow \text{P}$ ) and cleavage step ( $\text{D} \rightarrow \text{P}$ ) of  $[\text{L}_3\text{M}-\text{CN}-\text{M}'\text{L}_3]$  ( $\text{L} = \text{NH}_2$ ) systems. Results correspond to  $C_{3v}$  symmetry

Metal Elements	Charge <sup>a</sup>	$\Delta E$ ( $\text{R} \rightarrow \text{P}$ ) <sup>b</sup>	$\Delta E$ ( $\text{D} \rightarrow \text{P}$ ) <sup>b</sup>	$\Delta G$ ( $\text{R} \rightarrow \text{P}$ ) <sup>c</sup>	$\Delta G$ ( $\text{D} \rightarrow \text{P}$ ) <sup>c</sup>
Tc, Mo	0	–317	+90	–263	+42
Re, W	0	–475	–18	–417	–63
Bh, Sg	0	–487	–89	–433	–150
Mo, Mo	–1	–222	+32	–163	–10
W, W	–1	–391	–67	–337	–118
Sg, Sg	–1	–417	–135	–363	–192
Nb, Nb <sup>d</sup>	–3	–306	–104	–255	–158
Ta, Ta	–3	–463	–156	–412	–208
Ti, Ti	–5	–345	–137	–292	–185

<sup>a</sup> This value corresponds to the overall charge of the  $[\text{L}_3\text{M} + \text{CN} + \text{M}'\text{L}_3]$  system and is also equal to the molecular charge on the dinuclear species.

<sup>b</sup> The bonding energy was calculated as the electronic energy at 0.0 K corrected for zero-point effects. <sup>c</sup> The free energy was calculated at 298.15 K and 1.0 atm. <sup>d</sup> Due to technical difficulties associated with calculations using  $C_{3v}$  symmetry, results for this system correspond to  $C_s$  symmetry but with the  $[\text{Nb}-\text{CN}-\text{Nb}]$  core constrained to remain in a linear configuration throughout the calculation.

in the isolated ion case, whereas in the Ta complex (from the 5d series and group 5) the analogous bond lengthening is ~9 pm.

Largely similar trends are found for the  $[\text{L}_3\text{M}-\text{CN}-\text{ML}_3]$  dinuclear species, as shown in Table 2, in which the C–N distances obtained for both spin singlet ( $S = 0$ ) and triplet ( $S = 1$ ) states are included. For corresponding systems, a comparison of the C–N bond lengths in the encounter complexes and dinuclear species reveals a greater degree of activation in the latter due to enhancement of the  $\text{M}(d_{\pi})$ -to- $\text{CN}(\pi^*)$  back-donation when two metal–cyanide interactions are present.

Thermochemical parameters for the overall reaction and C–N cleavage step are presented in Table 3, where the results are given

in terms of both free energy and bonding energy, as the latter may be more easily correlated with electronic structure properties. Nevertheless, for the systems included in this study, the general trends are qualitatively similar, irrespective of which parameter is considered.

For the overall reaction, all cases investigated exhibit favourable energetics, but the bonding energy and free energy changes are of significantly greater magnitude in 5d relative to 4d systems, whereas a comparatively smaller difference is found between 5d and 6d systems. Overall, within a given group, a consistent trend is observed in that the energetics become increasingly favourable as the group is descended. In contrast, results are more variable across periods, with values for systems from groups 5 and 7 being similar but greater than those corresponding to systems from group 6.

For the C–N cleavage step, the general trends within individual groups are analogous to those found for the overall reaction, with more favourable energetics predicted for heavier relative to lighter members. However, unlike the variable results obtained in the overall reaction case, the general trends across periods are in the form of increasingly favourable energetics (for C–N cleavage) in the case of earlier relative to later members.

In terms of the free energy results for individual systems, cleavage of the C–N bond in the dinuclear species is predicted not to be favourable for  $[L_3Tc-CN-MoL_3]$ , and only slightly favourable for  $[L_3Mo-CN-MoL_3]^{(-)}$ , but in all other cases investigated, C–N bond scission, with subsequent formation of the carbide and nitride products, appears to be a thermodynamically favourable process.

Within the 4d and 5d series, the most favourable results are found for the systems from group 5, with values of  $-158$  and  $-208$  kJ mol $^{-1}$  for the C–N cleavage step ( $[\Delta G(D \rightarrow P)]$  in Table 3) in the case of Nb and Ta, respectively. However, in addition to thermodynamic factors, it is necessary to consider reaction barriers, which are predicted to be (from the potential energy scans shown in the supplementary information†) 197 kJ mol $^{-1}$  for the Nb system and 113 kJ mol $^{-1}$  for the Ta system. It is worth noting that the latter value is relatively close to the experimentally determined activation enthalpy of 96 kJ mol $^{-1}$  for the  $[Mo-NN-Mo]$  system that undergoes N–N bond cleavage at ambient conditions.<sup>10</sup> Furthermore, since some degree of structural distortion, leading to energetic stabilization, is likely to occur in the transition state, the cleavage barrier in the  $[Ta-CN-Ta]$  system could be even closer to, and possibly lower than, that of the  $[Mo-NN-Mo]$  analogue.

**3.3.2 Correlation with electronic structure properties.** In previous investigations,<sup>7,20</sup> we have conducted comparative bonding analyses of dinitrogen, carbon monoxide, cyanide, and nitric oxide activation by transition metal complexes, through fragment and energy decomposition approaches. These bonding analyses have shown that the  $\pi$  interactions between the metal (M or M') and small molecule ( $X^1-X^2$ ) fragments play an appreciably greater role than the corresponding  $\sigma$  interactions in the activation of the  $X^1-X^2$  bond. Furthermore, these results, in conjunction with related computational work,<sup>44,48</sup> suggest that optimization of the  $\pi$  interactions is central to increasing the ability of the dinuclear metal  $[L_3M-X^1X^2-M'L_3]$  systems to activate and cleave multiple bonds in small molecules.

For the specific case of cyanide, which can be described as possessing a chemical bond that is more resistant to cleavage

**Table 4** Energy gaps between the relevant  $\sigma$ -like  $[\Delta E(\sigma)]$  and  $\pi$ -like  $[\Delta E(\pi)]$  fragment orbitals in  $[L_3M-CN-M'L_3]$  ( $L = NH_2$ ) species. Calculations were performed on structures in which the M–C and N–M' distances were fixed at 400 pm. Results correspond to  $C_3v$  symmetry

Metal Elements	Molecular Charge	$\Delta E(\sigma)/eV^a$	$\Delta E(\pi)/eV^a$
Tc, Mo	0	0.78, 1.69	6.95, 4.36
Re, W	0	0.98, 1.49	6.51, 3.90
Bh, Sg	0	0.11, 1.26	5.73, 3.38
Cr, Cr	-1	1.56, 1.51	4.85, 4.84
Mo, Mo	-1	1.79, 1.69	4.40, 4.43
W, W	-1	1.67, 1.51	3.82, 3.87
Sg, Sg	-1	1.52, 1.31	3.19, 3.26
V, V	-3	3.68, 3.56	2.03, 2.09
Nb, Nb	-3	3.33, 3.17	1.98, 2.02
Ta, Ta	-3	3.04, 2.90	1.50, 1.40
Ti, Ti	-5	4.17, 3.99	0.85, 0.53

<sup>a</sup> Values correspond to M–CN, CN–M' interaction, respectively.

than that of dinitrogen, carbon monoxide, and nitric oxide, previous investigations<sup>7,20</sup> have revealed that the energy match between the  $\pi$ -like orbitals on the metal-based and small-molecule fragments, and also the magnitude of the corresponding fragment orbital interactions, are less favourable than in any of the other  $[L_3M-X^1X^2-M'L_3]$  ( $X^1-X^2 = N-N, C-O, N-O$ ) systems studied.

Spatial plots of the most significant  $\sigma$  and  $\pi$  orbital interactions across the  $[M-CN-M']$  unit are shown in Fig. 5 for the 4d and 5d series. The percentage contributions to the orbital compositions, given by the numbers in parentheses in Fig. 5, provide an indication of the amount of orbital mixing at the equilibrium geometry, and the most significant trends, in relation to C–N activation and cleavage, are associated with an increase in M–C  $\pi$ -like orbital mixing in complexes containing earlier and heavier elements.

In Table 4, the energy gaps between the relevant  $\sigma$ -like  $[\Delta E(\sigma)]$  and  $\pi$ -like  $[\Delta E(\pi)]$  fragment orbitals on the  $[ML_3]$  and  $[CN]$  moieties are given for all species included in this work. These results have been obtained from calculations in which the M–C and N–M' bonds were fixed at a sufficiently long distance (specifically 400 pm) so that orbital mixing between the terminal  $[ML_3]$  and central  $[CN]$  fragments is negligible. The general trends indicate that for groups 6 and 7, the energy match between the metal-based and cyanide fragment orbitals is more favourable for  $\sigma$  than  $\pi$  interactions, whereas the reverse observation applies to groups 4 and 5. Also, a decrease in the magnitude of the  $\pi$  orbital gaps is found for the earlier relative to later members across periods, and for the heavier relative to lighter members within groups. All of these results show strong correlation with both the degree of C–N activation in the dinuclear species and the energetics of the C–N bond cleavage step.

**3.3.3 Selected results for  $[NMe_2]$  systems.** In addition to the comparison of the three Mo ( $[NH_2]$ ,  $[NMe_2]$ ,  $[N^iPrPh]$ ) systems presented in Section 3.2, calculations have also been performed on a number of  $[NMe_2]$  cases involving other 4d and 5d transition metals in order to further examine the effects of changes in ligand identity and geometry of the dinuclear species on the C–N cleavage energetics. Since convergence of both electronic structure and geometry is considerably more difficult to achieve for these species,

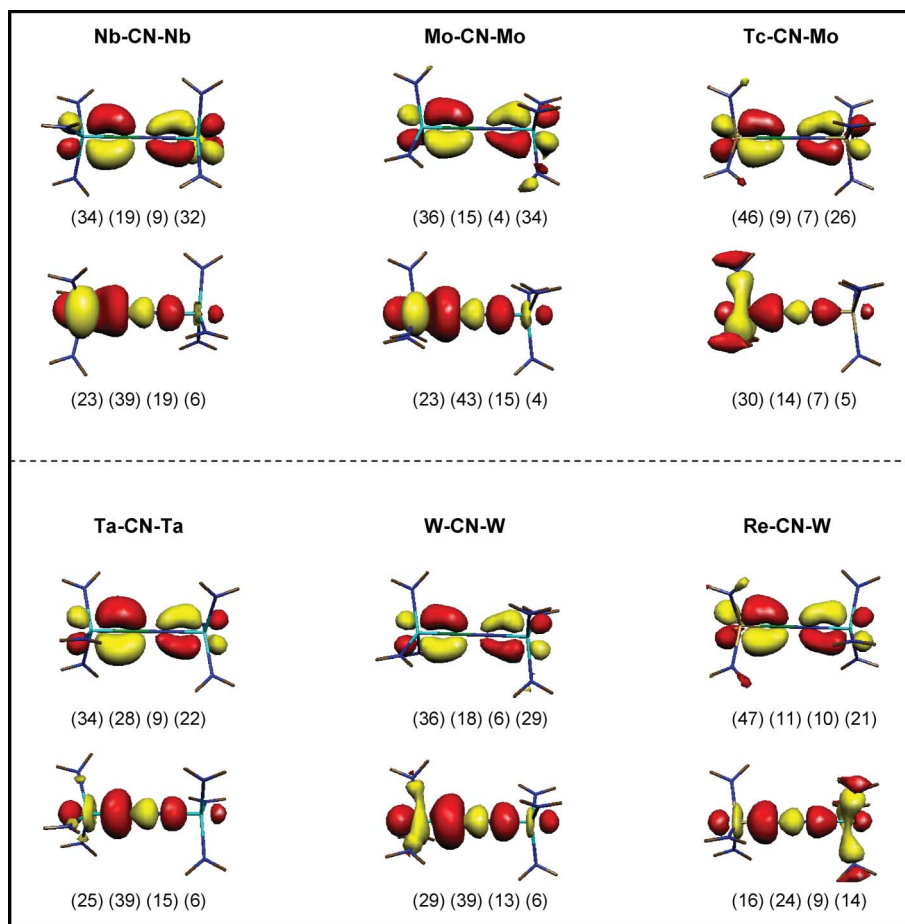


**Fig. 5** Spatial plots of the most significant  $\sigma$  and  $\pi$  orbital interactions across the  $[M-CN-M']$  unit in 4d and 5d metal systems. The numbers in parentheses indicate the contribution (percentage) from the M, C, N, and  $M'$  atoms to the composition of the orbital.

due to the lower symmetry and increased chemical complexity compared to the corresponding  $[NH_2]$  analogues, only the 4d (Nb, Mo, Tc) series and the overall uncharged  $[Re-CN-W]$  member of the 5d series have been investigated.

Results in the form of free energy reaction profiles are summarized in Fig. 6 and, in general, display similar trends to those observed for the  $[NH_2]$  systems. In all cases, the overall reaction is characterized by favourable energetics and, for the C–N cleavage step, a comparison of the analogous combinations from groups 6 and 7 indicates a significantly more facile process (by 166  $\text{kJ mol}^{-1}$ ) for the 5d  $[Re-CN-W]$  compared to 4d  $[Tc-CN-Mo]$  system. In addition, the typical trend of increasingly favourable energetics for the earlier relative to later members of a period is found across the 4d (Nb, Mo, Tc) series.

As shown in Scheme 1, the structure of  $[(NMe_2)_3Mo-CN-Mo(NMe_2)_3]^{(-)}$  exhibits significant distortions from the  $C_{3v}$  geometry of the  $[NH_2]$  analogue, and is predicted to be more stable in the singlet than triplet state. These characteristics are also observed in the analogous  $[(NMe_2)_3Nb-CN-Nb(NMe_2)_3]^{(3-)}$  and  $[(NMe_2)_3Tc-CN-Mo(NMe_2)_3]$  complexes. However, in the case of the  $[Re-CN-W]$  system, the optimized structure of the dinuclear species remains close to ideal  $C_{3v}$  symmetry and the triplet state is energetically favoured over the singlet state.

A comparison of selected properties of the dinuclear species for the  $[NH_2]$  and  $[NMe_2]$  systems is given in Table 5. All three

**Table 5** Comparison of selected properties of the dinuclear species in  $[Re-CN-W]$ ,  $[Tc-CN-Mo]$ ,  $[Mo-CN-Mo]$ , and  $[Nb-CN-Nb]$  systems with  $[NH_2]$  and  $[NMe_2]$  ligands

Metal Elements	Ligands <sup>a</sup>	Charge <sup>b</sup>	Spin State <sup>c</sup>	C–N <sup>d</sup>	$\Delta G$ (D→P) <sup>e</sup>	$\Delta E_s$ (D→P) <sup>f</sup>
Re, W	$NH_2$	0	$S = 1$	123.6	–63	–59
	$NMe_2$	0	$S = 1$	123.3	–106	–88
Tc, Mo	$NH_2$	0	$S = 1$	122.9	+42	–27
	$NMe_2$	0	$S = 0$	123.4	–4	–58
Mo, Mo	$NH_2$	–1	$S = 1$	125.0	–10	–84
	$NMe_2$	–1	$S = 0$	128.8	–55	–126
Nb, Nb	$NH_2$	–3	$S = 0$	130.6	–158	+286
	$NMe_2$	–3	$S = 0$	131.4	–141	+287

<sup>a</sup> Molecular symmetry is  $C_{3v}$  and  $C_1$  for  $[NH_2]$  and  $[NMe_2]$  systems, respectively. <sup>b</sup> This value corresponds to the overall charge of the  $[L_3M + CN + M'L_3]$  system and is also equal to the molecular charge on the dinuclear species. <sup>c</sup> Energetically most favourable spin state for the dinuclear species. <sup>d</sup> Bond distance in picometres (pm). <sup>e</sup> Free energy change (in  $\text{kJ mol}^{-1}$ ) for the dissociation of the dinuclear species into carbide and nitride products, calculated at 298.15 K and 1.0 atm. <sup>f</sup> Solvation energy change (in  $\text{kJ mol}^{-1}$ ) for the dissociation of the dinuclear species into carbide and nitride products.

members of the 4d series display a somewhat more activated C–N bond in the  $[NMe_2]$  system compared to the  $[NH_2]$  analogue, a result that can be attributed to the structural distortions

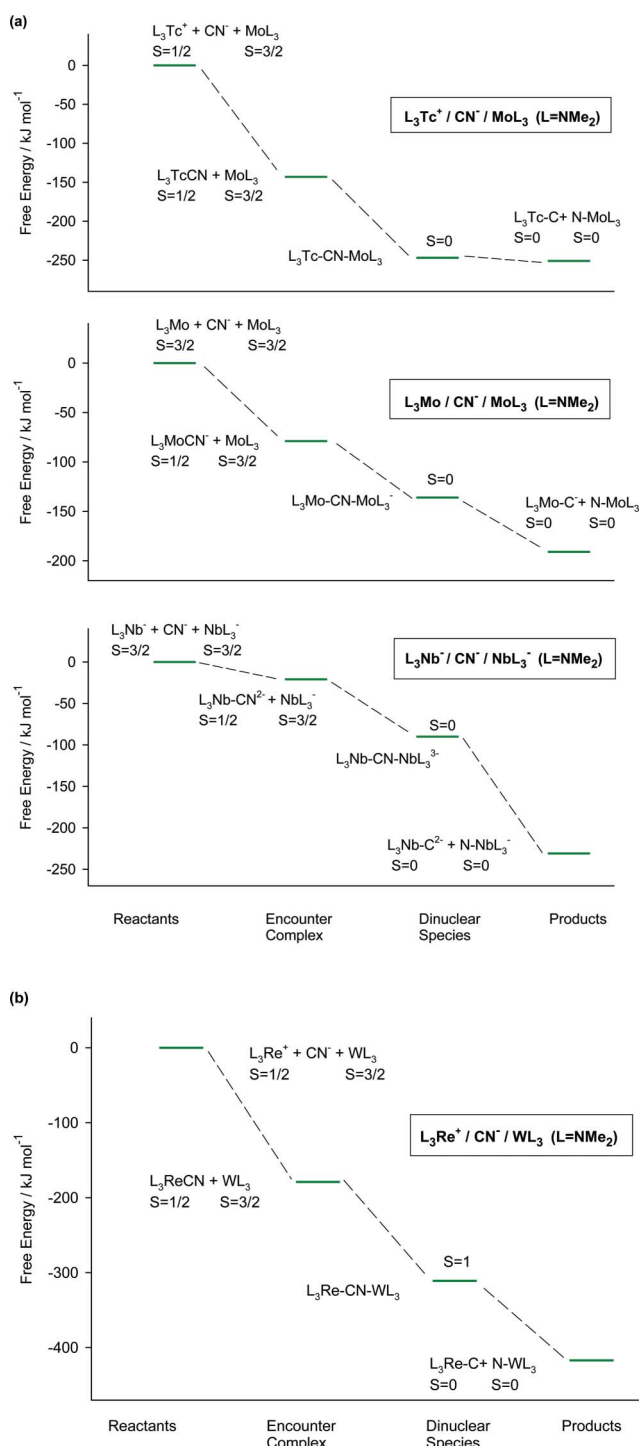


**Fig. 6** Comparison of reaction free energy profiles for selected  $[L_3M-CN-M'L_3]$  ( $L = [NMe_2]$ ) systems. All results correspond to  $C_1$  symmetry.

occurring when the molecular symmetry is relaxed from  $C_{3v}$  to  $C_1$ . However, in the  $[Re-CN-W]$  system, the structure of the dinuclear species does not undergo significant changes when its geometry is optimized without symmetry constraints, and the C–N distance is actually slightly shorter in the  $[NMe_2]$  ( $C_1$ ) than  $[NH_2]$  ( $C_{3v}$ ) case.

Examination of the C–N cleavage energetics indicates that scission of the C–N bond appears to be more favourable in

the  $[NMe_2]$  than  $[NH_2]$  systems, by 43, 46, and 45 kJ mol<sup>-1</sup> for  $[L_3Re-CN-WL_3]$ ,  $[L_3Tc-CN-MoL_3]$ , and  $[L_3Mo-CN-MoL_3]^{3-}$ , respectively. However, the reverse result is found for  $[L_3Nb-CN-NbL_3]^{3-}$ , although the difference between  $[NMe_2]$  and  $[NH_2]$  systems is comparatively smaller, with C–N bond scission being less favourable in the former by 15 kJ mol<sup>-1</sup>.

It is interesting to note that a correlation is apparent between trends in the C–N cleavage energetics and the corresponding solvation energy changes. In the  $[Re-CN-W]$ ,  $[Tc-CN-Mo]$ , and  $[Mo-CN-Mo]$  systems, most species are uncharged or carry a low negative charge, and solvation effects favour the products over the dinuclear species, but to a greater extent in the  $[NMe_2]$  than  $[NH_2]$  case. In contrast, the analogous results for the  $[Nb-CN-Nb]$  system, in which most species carry a relatively high negative charge, indicate that the dinuclear species is favoured over the products, and almost identical solvation energy values have been obtained for the  $[NMe_2]$  and  $[NH_2]$  cases.

Given that solvent models are highly sensitive to the magnitude of the molecular charge (as shown by the absolute values in Table 5), a possible explanation for the observed differences may be attributed to the fact that, in the  $[Nb-CN-Nb]$  system, the high negative charge could be the dominant factor in the interactions with the solvent, whereas for the remaining systems, other properties such as surface area may play a more important role.

**3.3.4 Selected results for  $[N^iPrPh]$  systems.** Although the overall results and trends obtained in the study of the C–N cleavage process in  $[L_3M-CN-M'L_3]$  systems across various transition metal periods and groups has indicated that Ta complexes represent the most favourable choice for achieving scission of the C–N bond, these results are limited to the  $[NH_2]$  case. Therefore, in order to confirm these observations—albeit at a necessarily more approximate level of calculation—it is convenient to consider additional results obtained for the more realistic  $[L_3Ta-CN-TaL_3]$  system in which the larger  $[N^iPrPh]$  ligands are used (Fig. 7).

Since a complete thermochemical and mechanistic analysis is not feasible in the  $[N^iPrPh]$  case, the comparison between this system and the simple  $[NH_2]$  analogue is limited to reaction profiles generated using bonding energy instead of free energy results. Nevertheless, general similarities on both qualitative and semi-quantitative levels are observed, with the  $[(N^iPrPh)_3Ta-CN-Ta(N^iPrPh)_3]^{3-}$  species possessing a spin singlet ground state and the cleavage step being favourable by 79 kJ mol<sup>-1</sup>.

Moreover, as entropic effects should favour the products over the dinuclear species, it is reasonable to conclude that scission of the C–N bond in  $[(N^iPrPh)_3Ta-CN-Ta(N^iPrPh)_3]^{3-}$  is likely to be clearly favourable on thermodynamic grounds. Also, as mentioned in Section 3.3.1, extrapolation of the results obtained for  $[(NH_2)_3Ta-CN-Ta(NH_2)_3]^{3-}$  suggests that the barrier to C–N cleavage could be close to, or lower than, that of the experimentally characterized  $[Mo-NN-Mo]$  system that undergoes N–N bond scission at ambient conditions.<sup>10</sup>

**3.3.5 Comment on results for special cases.** The general results discussed in this work are based primarily on an analysis of 4d and 5d metal systems, but calculations involving species that contain 3d and 6d transition elements have also been included in this study, since these results provide confirmation, on a conceptual basis, of the overall periodic trends, even though the

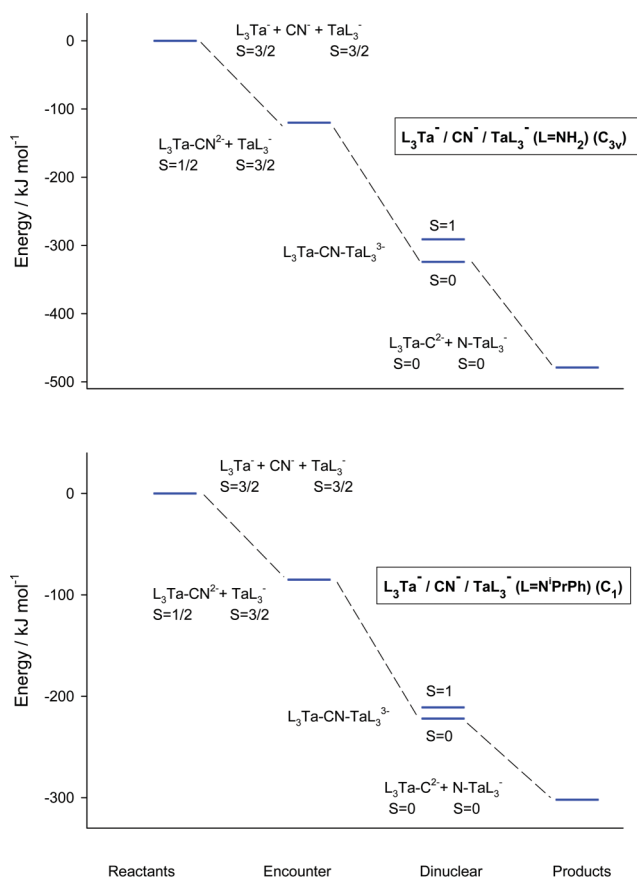


**Fig. 7** Comparison of reaction energy profiles for [Ta–CN–Ta] systems with [NH<sub>2</sub>] and [N<sup>i</sup>PrPh] ligands.

specific [Ti–CN–Ti], [Sg–CN–Sg], and [Bh–CN–Sg] systems are unrealistic from a strictly practical viewpoint.

Within groups 6 and 7, the results obtained for the 6d systems confirm the general trend that increasingly favourable energetics are observed for the heavier members due to the energy gaps between relevant  $\pi$ -like orbitals on the metal-based and cyanide fragments becoming smaller as the groups are descended.

In the case of the Ti system, the fact that the formal oxidation state of the Ti atoms is +1 and the overall negative charge on the [L<sub>3</sub>Ti–CN] and [L<sub>3</sub>Ti–CN–TiL<sub>3</sub>] molecules has a notably large value (of –3 and –5, respectively) results in particularly high-lying metal  $d_{\pi}$  orbitals that are energetically close to the cyanide  $\pi^*$  levels. Consequently, these species exhibit the greatest degree of C–N activation and the closest energy match between  $\pi$ -like fragment orbitals among all [L<sub>3</sub>M–CN] and [L<sub>3</sub>M–CN–M'L<sub>3</sub>] complexes considered in this study, and the C–N cleavage process is characterized by highly favourable energetics.

## 4 Conclusion

Calculations employing density functional theory have been conducted to investigate C–N bond activation and cleavage in dinuclear metal–cyanide [L<sub>3</sub>M–CN–M'L<sub>3</sub>] systems in which the metal sites are transition elements from the 3d, 4d, 5d, or 6d series and groups 4 through 7, whilst the amide ligands are either [NR<sub>2</sub>] (R = H, Me) or [NRAr] (R = <sup>i</sup>Pr, Ar = Ph). The effects

of including homonuclear and heteronuclear metal combinations, and changing overall molecular charge, nature of the ligands, and dinuclear intermediate geometry (through relaxation of symmetry constraints), on the thermodynamic and mechanistic aspects of the C–N cleavage process have been explored. We have proposed a possible explanation for the failure of the molybdenum-based experimental system to achieve C–N bond scission, and we have found a novel result in that a tantalum-based system should, in principle, be capable of cleaving the cyanide molecule under relatively mild conditions.

A comparative analysis of [L<sub>3</sub>Mo–CN–MoL<sub>3</sub>] systems with L = [NH<sub>2</sub>], [NMe<sub>2</sub>], or [N<sup>i</sup>PrPh], which are of particular interest due to their experimental relevance, has shown that, irrespective of the nature of the amide ligand and overall molecular symmetry ( $C_{3v}$  or  $C_1$ ), the C–N cleavage step is, in enthalpy terms, endothermic even though the overall reaction is highly exothermic. However, since entropy effects favour the carbide and nitride products over the dinuclear species, cleavage of the C–N bond is predicted to be a favourable process on the basis of relative free energy considerations. The fact that competing reactions, such as ejection of an [R] group, are observed experimentally instead of C–N bond scission, is likely to be a consequence of a rather large barrier associated with the dissociation of [L<sub>3</sub>Mo–CN–MoL<sub>3</sub>]<sup>(-)</sup> into [L<sub>3</sub>Mo–C]<sup>(-)</sup> and [N–MoL<sub>3</sub>], which is predicted to be in the vicinity of 190 kJ mol<sup>-1</sup>.

The general trends in C–N bond lengths and cleavage energetics reveal a greater degree of activation and more favourable thermochemical conditions for the heavier relative to lighter members within a group, and for the earlier relative to later members within a period. These trends are analogous to the observed periodic variations in the strength of metal–element bonds in the products (M–C and M–N in the cyanide case), which are considered to be the thermodynamic driving force for the cleavage of multiply-bonded small molecules. Furthermore, the trends in C–N bond distance and cleavage energetics are strongly correlated with the energetic separation of the  $\pi$  orbitals on the metal-based and cyanide fragments, with the most favourable results for C–N bond scission found for systems exhibiting the closest match between the relevant ( $\pi$ -like) fragment orbitals.

A significant implication from these structural, bonding, and thermochemical trends is that the tris-amide molybdenum complexes used in the experimental systems are not particularly well suited to cleaving the C–N bond in cyanide due to relatively unfavourable interactions between the fragment orbitals that play a central role in the activation and cleavage of multiply-bonded small molecules.

Since the aforementioned trends favour the earlier and heavier members of the d block, tantalum species have emerged as those best suited to cleaving the C–N bond in dinuclear metal–cyanide complexes. The [Ta–CN–Ta] system exhibits the most favourable energetics for the C–N bond scission step and the barrier to C–N cleavage has been calculated to be close in magnitude to that experimentally determined for the analogous N–N bond scission in dinuclear metal–dinitrogen complexes.

Although in the tantalum case, and also for other metal systems examined in this study, the reaction with cyanide involves species carrying a relatively high negative charge that could render their handling under experimental conditions difficult, an important conclusion from our computational investigations lies in the

fact that cleavage of multiply-bonded, and relatively unreactive, molecular fragments may be achieved through the tuning of electronic structure and orbital interactions by judicious choice of metal sites and ligand groups.

## Acknowledgements

The authors acknowledge financial support from the Australian Research Council and access to the Australian National University supercomputer facilities of the National Computational Infrastructure.

## References

- 1 K. R. Dunbar and R. A. Heintz, *Prog. Inorg. Chem.*, 1997, **45**, 283.
- 2 W. P. Fehlhammer and M. Fritz, *Chem. Rev.*, 1993, **93**, 1243.
- 3 P. V. Bernhardt, F. Bozoglian, B. P. Macpherson and M. Martinez, *Coord. Chem. Rev.*, 2005, **249**, 1902.
- 4 S. Tanase and J. Reedijk, *Coord. Chem. Rev.*, 2006, **250**, 2501.
- 5 M. Berrettoni, M. Giorgetti, S. Zamponi, P. Conti, D. Ranganathan, A. Zanotto, M. L. Saladino and E. Caponetti, *J. Phys. Chem. C*, 2010, **114**, 6401.
- 6 J. C. Peters, L. M. Baraldo, T. A. Baker, A. R. Johnson and C. C. Cummins, *J. Organomet. Chem.*, 1999, **591**, 24.
- 7 G. Christian, R. Stranger, B. F. Yates and C. C. Cummins, *Dalton Trans.*, 2008, 338.
- 8 K.-H. Tryluszka, A. Schröder, I. Brüdgam, R. Thiel and W. P. Fehlhammer, *Inorg. Chim. Acta*, 1998, **269**, 23.
- 9 C. E. Laplaza and C. C. Cummins, *Science*, 1995, **268**, 861.
- 10 C. E. Laplaza, M. J. A. Johnson, J. C. Peters, A. L. Odom, E. Kim, C. C. Cummins, G. N. George and I. J. Pickering, *J. Am. Chem. Soc.*, 1996, **118**, 8623.
- 11 C. C. Cummins, *Chem. Commun.*, 1998, 1777.
- 12 J.-P. F. Cherry, A. R. Johnson, L. M. Baraldo, Y.-C. Tsai, C. C. Cummins, S. V. Kryatov, E. V. Rybak-Akimova, K. B. Capps, C. D. Hoff, C. M. Haar and S. P. Nolan, *J. Am. Chem. Soc.*, 2001, **123**, 7271.
- 13 A. L. Odom, C. C. Cummins and J. D. Protasiewicz, *J. Am. Chem. Soc.*, 1995, **117**, 6613.
- 14 J. C. Peters, A. L. Odom and C. C. Cummins, *Chem. Commun.*, 1997, 1995.
- 15 J. B. Greco, J. C. Peters, T. A. Baker, W. M. Davis, C. C. Cummins and G. Wu, *J. Am. Chem. Soc.*, 2001, **123**, 5003.
- 16 Y.-C. Tsai, M. J. A. Johnson, D. J. Mindiola and C. C. Cummins, *J. Am. Chem. Soc.*, 1999, **121**, 10426.
- 17 A. R. Johnson, W. M. Davis, C. C. Cummins, S. Serron, S. P. Nolan, D. G. Musaev and K. Morokuma, *J. Am. Chem. Soc.*, 1998, **120**, 2071.
- 18 G. J. Christian, R. Stranger and B. F. Yates, *Inorg. Chem.*, 2006, **45**, 6851.
- 19 G. Cavigliasso, L. Wilson, S. McAlpine, M. Attar, R. Stranger and B. F. Yates, *Dalton Trans.*, 2010, 4529.
- 20 G. Cavigliasso, G. Christian, R. Stranger and B. F. Yates, *Dalton Trans.*, 2009, 956.
- 21 G. Christian, R. Stranger, S. Petrie, B. F. Yates and C. C. Cummins, *Chem.–Eur. J.*, 2007, **13**, 4264.
- 22 G. Christian, R. Stranger, B. F. Yates and C. C. Cummins, *Eur. J. Inorg. Chem.*, 2007, 3736.
- 23 N. J. Brookes, A. Ariafard, R. Stranger and B. F. Yates, *Dalton Trans.*, 2009, 9266.
- 24 N. J. Brookes, A. Ariafard, R. Stranger and B. F. Yates, *Chem. Eur. J.*, 2010, **16**, 8117.
- 25 A. Ariafard, N. J. Brookes, R. Stranger and B. F. Yates, *J. Am. Chem. Soc.*, 2008, **130**, 11928.
- 26 Amsterdam Density Functional, Scientific Computing and Modelling, Theoretical Chemistry, Vrije Universiteit, Amsterdam, The Netherlands (<http://www.scm.com>).
- 27 C. Fonseca Guerra, J. G. Snijders, G. te Velde and E. J. Baerends, *Theor. Chem. Acc.*, 1998, **99**, 391.
- 28 G. te Velde, F. M. Bickelhaupt, S. J. A. van Gisbergen, C. Fonseca Guerra, E. J. Baerends, J. G. Snijders and T. Ziegler, *J. Comput. Chem.*, 2001, **22**, 931.
- 29 A. D. Becke, *Phys. Rev. A: At., Mol., Opt. Phys.*, 1988, **38**, 3098.
- 30 J. P. Perdew, *Phys. Rev. B*, 1986, **33**, 8822.
- 31 E. van Lenthe, E. J. Baerends and J. G. Snijders, *J. Chem. Phys.*, 1993, **99**, 4597.
- 32 E. van Lenthe, E. J. Baerends and J. G. Snijders, *J. Chem. Phys.*, 1994, **101**, 9783.
- 33 E. van Lenthe, A. E. Ehlers and E. J. Baerends, *J. Chem. Phys.*, 1999, **110**, 8943.
- 34 C. C. Pye and T. Ziegler, *Theor. Chem. Acc.*, 1999, **101**, 396.
- 35 L. Y. Fan and T. Ziegler, *J. Chem. Phys.*, 1992, **96**, 9005.
- 36 L. Y. Fan and T. Ziegler, *J. Phys. Chem.*, 1992, **96**, 6937.
- 37 MOLEKEL: An Interactive Molecular Graphics Tool (<http://www.cscs.ch/molekel/>).
- 38 S. Portmann and H. P. Lüthi, *Chimia*, 2000, **54**, 766.
- 39 MOLDEN: A Pre and Post Processing Program for Molecular and Electronic Structures (<http://www.cmbi.ru.nl/molden/molden.html>).
- 40 G. Schaftenaar and J. H. Noordik, *J. Comput.-Aided Mol. Des.*, 2000, **14**, 123.
- 41 P. J. Stephens, F. J. Devlin, C. F. Chabalowski and M. J. Frisch, *J. Phys. Chem.*, 1994, **98**, 11623.
- 42 N. J. Brookes, D. C. Graham, G. Christian, R. Stranger and B. F. Yates, *J. Comput. Chem.*, 2009, **30**, 2146.
- 43 J. J. Curley, T. R. Cook, S. Y. Reece, P. Müller and C. C. Cummins, *J. Am. Chem. Soc.*, 2008, **130**, 9394.
- 44 G. Christian, R. Stranger, B. F. Yates and D. C. Graham, *Dalton Trans.*, 2005, 962.
- 45 G. Christian, J. Driver and R. Stranger, *Faraday Discuss.*, 2003, **124**, 331.
- 46 R. K. Hocking, R. J. Deeth and T. W. Hambley, *Inorg. Chem.*, 2007, **46**, 8238.
- 47 G. Cavigliasso, R. Stranger, L. F. McClintock, S. E. Cheyne, P. M. Jaffray, K. E. Baxter and A. G. Blackman, *Dalton Trans.*, 2008, 2433.
- 48 A. Ariafard, N. J. Brookes, R. Stranger and B. F. Yates, *Chem.–Eur. J.*, 2008, **14**, 6119.